

# Polymorph of 2,9-Dichloroquinacridone and Its Electronic Properties

Takatoshi Senju,\* Naoko Nishimura, and Jin Mizuguchi

Department of Applied Physics, Graduate School of Engineering, Yokohama National University, 79-5 Tokiwadai, Hodogaya-ku, 240-8501 Yokohama, Japan

Received: October 31, 2006; In Final Form: February 13, 2007

The title compound (2,9-DCIQA) is a hydrogen-bonded, bluish-red pigment. However, red and black single crystals have been isolated from the vapor phase in the higher- and lower-temperature regions around 380 and 150 °C, respectively. Because of this, correlation has been studied in the present investigation on the crystal structure and the shade in the solid state. The red phase is found to correspond to the commercial product as characterized by two-dimensional NH...O hydrogen bonds between the NH group of one molecule and the O atom of the neighboring one. On the other hand, the molecule of the black phase is heavily deformed and no intermolecular hydrogen bonds are recognized. The molecular distortion induced by crystallization in the black phase is found to displace the absorption band toward longer wavelengths to bring about the black color. In addition, the black phase is observed to be transformed into the red one around 200 °C.

## 1. Introduction

2,9-Dichloroquinacridone (2,9-DCIQA; Figure 1) is an industrially important red pigment (Pigment Red 202) which belongs to the class of hydrogen-bonded pigments.<sup>1</sup> The intermolecular hydrogen bonds hold the pigment molecules firmly together so as to impart a polymer-like stability. Therefore, the hydrogen-bonded pigments are extremely resistant to heat and light irradiation.<sup>1–4</sup> The hydrogen bonds are also important to displace the absorption bands toward longer wavelengths on going from solution to the solid state.<sup>2–4</sup>

2,9-DCIQA is practically used in painting and imaging industries together with 2,9-dimethyl derivative (2,9-DMQA; Pigment Red 122). Both materials are equally stable against heat and light irradiation. However, the former exhibits more bluish and duller shade than the latter, although no significant difference is recognized in molecular spectra in solution. In this connection, we initiated our investigation on the electronic structure of both compounds on the basis of the crystal structure in order to elucidate the difference in shade. We started with the structure analysis of 2,9-DMQA<sup>5</sup> and found that there is a two-dimensional intermolecular NH...O hydrogen-bond network, quite contrary to the three-dimensional network of unsubstituted  $\gamma$ -QA.<sup>6</sup> Furthermore, a large bathochromic shift is observed on going from solution to the solid state, as brought about by interactions between transition dipoles arranged in a “head-to-tail” fashion.<sup>2,4</sup> Then we tackled the structure of 2,9-DCIQA and found two crystalline phases (i.e., red<sup>7</sup> and black<sup>8</sup>) isolated from the vapor phase in the higher and lower temperature regions, respectively.

The objective of the present investigation is primarily to characterize the electronic structure of the red and black phases of 2,9-DCIQA on the basis of the crystal structure and secondarily to elucidate the difference in shade in the solid state between the red phase of 2,9-DCIQA and 2,9-DMQA.

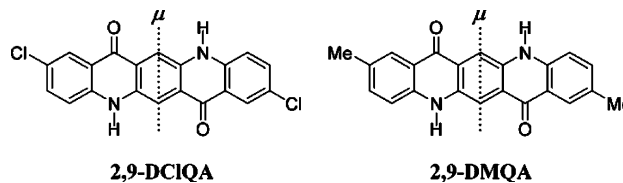


**Figure 1.** Molecular structure of 2,9-DCIQA and 2,9-DMQA. The direction of the transition dipoles ( $\mu$ ) is designated by dotted lines.

## 2. Experimental Section

**2.1. Materials and Crystal Growth.** 2,9-DCIQA and 2,9-DMQA were obtained from Dainippon Ink and Chemicals, Inc., and Ciba Specialty Chemicals, Inc., respectively. The samples were purified three times by sublimation, using a two-zone furnace.<sup>9</sup> Single crystals of 2,9-DCIQA were grown from the vapor phase at about 495 °C. Tiny red platelet crystals were condensed at a high-temperature region around 380 °C, whereas a number of black needles were grown in the low-temperature region around 150 °C. On the other hand, single crystals of 2,9-DMQA were grown from the vapor phase at about 430 °C. A number of prismatic crystals were obtained after 17 h.

**2.2. Equipment and Measurements.** Solution spectrum in dimethyl sulfoxide (DMSO) was recorded on a UV-2400PC spectrophotometer (Shimadzu). Reflection spectra on single crystals were measured by means of a UMSP80 microscope–spectrophotometer (Carl Zeiss). An Epiplan Pol ( $\times 8$ ) objective was used together with a Nicol-type polarizer. Reflectivities were corrected relative to the reflection standard of silicon carbide. Differential scanning calorimetry (DSC) analysis was made on single crystals in air by means of a Thermo Plus 2 DSC-8230 from Rigaku at a heating rate of 5 °C/min. Scanning electron micrographs of the surface of the single crystals were taken using a VE-8800 from Keyence.

**2.3. Molecular Orbital Calculations.** Semiempirical molecular orbital (MO) calculations were performed using a Quantum CAChe ver. 3.2 program package,<sup>10</sup> which includes MOPAC version 94.10 and the ZINDO programs. The heat of

\* To whom correspondence should be addressed. Phone/Fax: +81 45 339 4320. E-mail: tsenju@ynu.ac.jp.

**TABLE 1: Crystallographic Parameters for the Red and Black Phases of 2,9-DCIQA as Well as for 2,9-DMQA**

	2,9-DCIQA		2,9-DMQA <sup>5</sup>
	red phase <sup>7</sup>	black phase <sup>8</sup>	
molecular formula	C <sub>20</sub> H <sub>10</sub> Cl <sub>2</sub> N <sub>2</sub> O <sub>2</sub>		C <sub>22</sub> H <sub>16</sub> N <sub>2</sub> O <sub>2</sub>
molecular weight	381.22		340.37
crystal system	triclinic	monoclinic	triclinic
space group	<i>P</i> 1	<i>P</i> 2 <sub>1</sub> / <i>c</i>	<i>P</i> 1
molecular symmetry	<i>C</i> <sub>i</sub>	<i>C</i> <sub>i</sub>	<i>C</i> <sub>i</sub>
<i>Z</i>	1	2	1
<i>a</i> (Å)	3.7919(11)	3.782(1)	3.865(3)
<i>b</i> (Å)	5.8314(16)	14.840(4)	6.372(3)
<i>c</i> (Å)	16.754(4)	12.942(3)	15.78(2)
$\alpha$ (°)	94.956(16)	—	93.94(6)
$\beta$ (°)	95.136(17)	91.93(2)	91.51(8)
$\gamma$ (°)	90.660(18)	—	100.00(6)
<i>V</i> (Å <sup>3</sup> )	366.56(17)	726.0(3)	381.5(6)
<i>D</i> <sub>x</sub> (Mg m <sup>-3</sup> )	1.727	1.744	1.481
<i>R</i> <sub>1</sub> ( <i>I</i> > 2 $\sigma$ ( <i>I</i> ))	0.056	0.100	0.056

formation and optical absorption bands of the molecules in the red and black phases were calculated on the basis of the *x*, *y*, and *z* X-ray coordinates for non-H atoms, while geometry were optimized for H atoms, using the AM1 Hamiltonian. Then spectroscopic calculations were made by the INDO/S Hamiltonian<sup>11</sup> including 196 singly excited configuration interactions composed of 14 occupied and 14 unoccupied MOs. In parallel, geometry optimization as well as spectroscopic computation was also performed for the molecule. This corresponds to the state in solution.

### 3. Results and Discussion

**3.1. Crystal Structure.** Table 1 lists the crystallographic parameters for the red<sup>7</sup> and black<sup>8</sup> phases of 2,9-DCIQA, together with those of 2,9-DMQA.<sup>5</sup> Panels a and b of Figure 2 show the top and side views of the molecular structure of the red and black phases of 2,9-DCIQA, respectively. The molecule in the red phase is nearly planar as characterized by the dihedral angle between the planes of rings A and B (178.6(1)°) and the one between the planes of rings A and C (179.2(1)°). This is in fairly good agreement with the optimized structure by semiempirical MO calculations. On the other hand, the molecule in the black phase is heavily deformed, especially around ring B, as shown in Figure 2b, as compared with that in the red phase. (The C/N bonds are  $r(\text{C5-N1}) = 1.39(1)$  and  $r(\text{C9-N1}) = 1.30(1)$  Å in the black phase; whereas  $r(\text{C5-N1}) = 1.369(4)$  and  $r(\text{C9-N1}) = 1.377(4)$  Å in the red phase.) As a result, the molecule is not entirely planar as indicated by the dihedral angles between the planes of rings A and B (177.9(3)°) and between the planes of rings A and C (176.7(3)°). This deformation in the black phase results in a higher heat of formation than in the red phase and has also significant influence on the absorption maximum as described in the next section.

Figure 3a,b shows the molecular arrangement of the red phase. The red phase is typically characterized by a two-dimensional hydrogen-bonded network. One molecule is hydrogen-bonded to two neighboring molecules through four hydrogen bonds. However, it should be noted that there is a step of about 0.55 Å between the molecular planes of two hydrogen-bonded molecules. The red phase is found to correspond to the commercial product (Pigment Red 202), as revealed from our X-ray powder diffraction analysis, and is also identified as the  $\gamma$ -modification of 2,9-DCIQA as claimed by Deuschel and others.<sup>12</sup> On the contrary, the molecular arrangement of the black phase is strikingly different as shown in Figure 4a,b. Furthermore, to our surprise, there are no NH $\cdots$ O

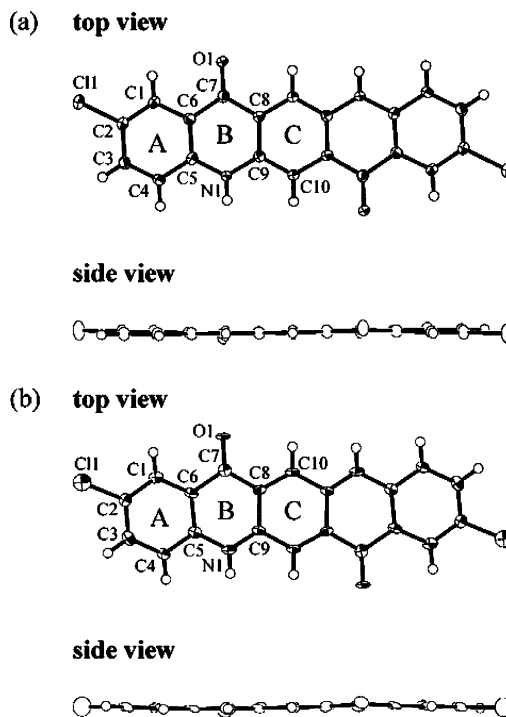


**Figure 2.** Molecular conformation of 2,9-DCIQA: (a) red phase and (b) black phase. Three six-membered rings are designated as A–C as shown in the figure.

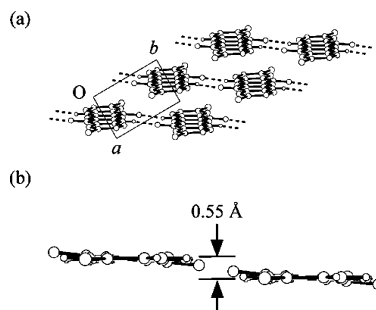


**Figure 3.** (a) Molecular arrangement of the red phase of 2,9-DCIQA. The dashed line designates the intermolecular hydrogen bond. (b) Two hydrogen-bonded molecules of 2,9-DCIQA showing the step of about 0.55 Å between the molecular planes.

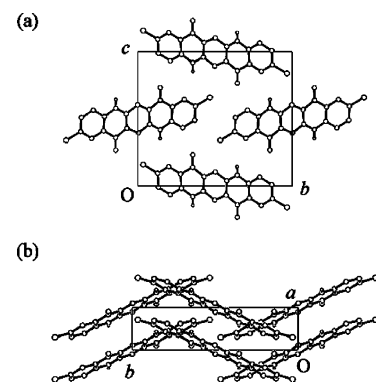


**Figure 4.** (a) The projection of the crystal structure of the black phase onto the (100) plane. (b) The projection of the crystal structure of the black phase onto the (001) plane.

intermolecular hydrogen bonds in the black phase that are usually observed in all hydrogen-bonded pigments.<sup>1</sup> (The N/O distance is 3.75 Å in the black phase while 2.87 Å in the red phase.) The molecules are arranged in a “hunter’s fence” fashion

**TABLE 2: Calculated Heat of Formation, HOMO and LUMO Levels, Absorption Maxima, and Their Oscillator Strength**

		$H_f$ (kJ/mol) <sup>a</sup>	HOMO (eV) <sup>a</sup>	LUMO (eV) <sup>a</sup>	$\Delta E_{\text{LUMO-HOMO}}$ (eV) <sup>a</sup>	$\lambda_{\text{max}}$ (nm) <sup>b</sup>	oscillator strength ( $f$ ) <sup>b</sup>
2,9-DCIQA	red phase (X-ray coord.)	74.00	-8.38	-1.30	7.08	371.6	0.29
	black phase (X-ray coord.)	153.57	-7.79	-1.11	6.68	414.8	0.32
	geo. opt.	50.44	-8.29	-1.21	7.08	371.9	0.28
2,9-DMQA	X-ray coord.	57.29	-8.04	-0.97	7.07	378.1	0.31

<sup>a</sup> AM1 Hamiltonian. <sup>b</sup> INDO/S Hamiltonian.

(*viz.* the molecules form a grid-like structure when viewed from the side) along the *a*-axis in the black phase (Figure 4b).

Then we turn our attention to the difference in structure between the red phase of 2,9-DCIQA<sup>7</sup> and 2,9-DMQA.<sup>5</sup> Basically, both structures are quite similar in molecular conformation as well as in molecular arrangement. However, a slight difference is observed in the step height between the molecular planes of two hydrogen-bonded molecules as shown in Figure 3(b): 0.55 Å in the red phase of 2,9-DCIQA and 0.87 Å in 2,9-DMQA. An even minor difference is also recognized in the center-to-center distance between the molecules: 6.91 and 6.85 Å for 2,9-DCIQA and 2,9-DMQA, respectively. Although the difference in step is quite small, this plays a non-negligible role in excitonic interactions that determine the difference in shade between 2,9-DCIQA and 2,9-DMQA in the solid state which will be discussed in section 3.4.

**3.2. Semiempirical MO Calculations.** Semiempirical MO calculations were carried out in order to study the influence of the molecular distortion on the heat of formation (i.e., stability) and the absorption bands of the molecule. The results are summarized in Table 2. It is remarkable to note that the heat of formation of the molecule in the red phase is considerably lower than that of the black phase by about 80 kJ/mol, but still higher than that of the geometry-optimized molecule by about 23.5 kJ/mol. Obviously, the molecular distortion in the black phase is responsible for the high heat of formation (i.e., less stable than the molecule in the red phase). Furthermore, the distortion is found to displace the absorption band toward longer wavelengths by about 43.2 nm (2803 cm<sup>-1</sup>) relative to that in the red phase. On the other hand, the absorption maxima of the molecule in the red phase and the geometry-optimized molecule appear at nearly the same wavelength, although the heat of formation is slightly different. No difference in oscillator strength is recognized between these three molecules (about 0.3). The direction of the transition dipole as deduced from the present calculation points perpendicular to the molecular axis and is shown in Figure 1.

**3.3. Electronic structure of 2,9-DCIQA.** **3.3.1. Solution Spectrum.** Figure 5 shows the solution spectrum for 2,9-DCIQA in dimethyl sulfoxide (DMSO). The absorption maximum occurs at 530 nm and a progression of the absorption bands is also observed, which starts from 530 nm toward shorter wavelengths. (2,9-DMQA gives a similar spectrum (not shown here), but the absorption maximum appears at 528 nm.) Since all absorption bands are equally spaced (about 1600 cm<sup>-1</sup>) and the absorption edge of the longest-wavelength band around 530 nm is steep,

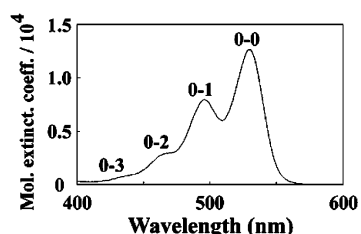


**Figure 5.** Solution spectrum of 2,9-DCIQA in DMSO.

the bands are typical of the vibronic transition, in which the pure electronic band (0–0 transition) is coupled with vibrational transitions: 0–1, 0–2, and 0–3 transitions as designated in Figure 5. This is also borne out by the MO calculations which shows one single  $\pi$ – $\pi^*$  electronic transition in the near UV region (Table 2) that is the longest-wavelength band.

**3.3.2. Solid-State Spectra.** Figure 6 shows the visible reflection spectra measured on single crystals by means of a microscope–spectrophotometer for the red and black phases of 2,9-DCIQA. The longest-wavelength band appears around 586 nm in the red phase while around 684 nm in the black phase: the difference of the reflection peaks amounts to 98 nm (2445 cm<sup>-1</sup>). It should also be noted that the spectral shape of the both spectra is quite similar to each other and is in fairly good accord with that of the solution spectrum (Figure 5). This indicates that the red and black spectra are merely caused by the bathochromic displacement on going from solution to the solid state.

It is also important to note that no noticeable difference in spectral shape of the reflection spectra is recognized between the red phase of 2,9-DCIQA and 2,9-DMQA (not shown here) and that the reflection maximum of the former appears at a slightly longer-wavelength than that of the latter by about 14 nm. This means that the red phase of 2,9-DCIQA is more bluish than 2,9-DMQA. The present difference in color between 2,9-DCIQA and 2,9-DMQA will be discussed in terms of excitonic interactions in the next section.

**3.4. Interactions between Transition Dipoles and the Role of NH···O Intermolecular Hydrogen Bonds.** As stated in introduction, the intermolecular hydrogen bonds bear two functions: stabilization of the system and bathochromic shifts.<sup>1–4</sup> The latter function is discussed here in terms of excitonic interactions which prevail in organic crystals, in which the component molecule has a high absorption coefficient and the molecules are periodically arranged. This situation is usually the case in dyestuffs and pigments.<sup>4,13–17</sup>

When an excitation induces a transition dipole in the molecule, the excited-state in crystals involves wavefunctions with significant probabilities on nearest neighbors. Therefore, the exciton coupling may well involve energy contributions from interactions with all of these nearest neighbor molecules acting in concert in the lattice. This may lead to a band splitting of the excited state, or spectral displacement toward longer wavelengths or shorter wavelengths. The interaction energy ( $\Delta E_{\text{exciton}}$ ) is given by the dipole–dipole equation:<sup>18,19</sup>  $\Delta E_{\text{exciton}}$

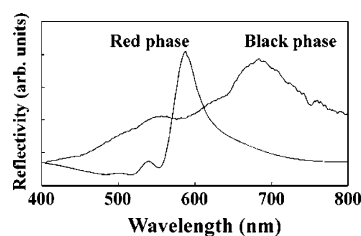


**Figure 6.** Reflection spectra in the visible region for the red and black phases of 2,9-DCIQA measured on single crystals.

$= |\mu|^2(1 - 3 \cos^2 \theta)/r^3$ , where  $\mu$  denotes the transition dipole,  $r$  the distance between two central points of two dipoles, and  $\theta$  the angle between the one dipole and the vector connecting the two point dipoles. As evident from the present equation, the overall spread or shift energy is determined by the strength of the interneighbor coupling ( $|\mu|^2$ ), which directly depends on the absorption coefficient of the molecule as well as the mutual relative orientation of the transition dipoles in molecular assemblies. That is, the term  $(1 - 3 \cos^2 \theta)$  determines the geometrical relationship of transition dipoles correlated with the crystal structure. The bathochromic or hypsochromic shift depends on the critical angle of  $\theta = 54.7^\circ$ , below which the former will result and above which the latter will be the case. The maximum bathochromic or hypsochromic shift is achieved by “head-to-tail”-arrangement or “parallel” arrangement, respectively.

First, we will discuss the difference in shade between the red phase of 2,9-DCIQA and 2,9-DMQA in terms of excitonic interactions on the basis of the hydrogen-bond pair as shown in Figure 3(b) (see section 3.1). The directions of the transition dipole for 2,9-DCIQA and 2,9-DMQA are given in Figure 1 (i.e., perpendicular to the long molecular axis) that are deduced from the MO calculations and also confirmed by experiment. Then, we notice that the hydrogen-bond pair forms a *quasi* “head-to-tail” arrangement that displaces most the absorption band toward longer wavelengths, although there is a small step between two hydrogen-bonded pairs: 0.55 Å in 2,9-DCIQA and 0.87 Å in 2,9-DMQA. The present difference in step height determines how the “head-to-tail” arrangement is perfect and thus exerts an influence on the extent of the bathochromic shift. Clearly, the smaller step height is advantageous to the bathochromic shift. This suggests that the absorption maximum in 2,9-DCIQA is expected to appear at longer wavelengths than in 2,9-DMQA. In fact, the former maximum occurs at longer wavelength by 14 nm than the latter (see section 3.3.2). This also explains why 2,9-DCIQA is more bluish red than 2,9-DMQA.

Next, we will consider the spectral shift on going from solution to the solid state in the red and black phases as shown in Figures 5 and 6. Here again, in the red phase, the  $\text{NH}\cdots\text{O}$  hydrogen-bond aligns the transition dipoles nearly in a “head-to-tail” fashion, causing the absorption band to occur around 580 nm. On the contrary, the absorption maximum in the black phase appears around 690 nm. This is primarily due to the molecular distortion (section 3.2) and secondarily to interactions between transition dipoles which are favorably arranged in a “quasi head-to-tail” fashion, although no  $\text{NH}\cdots\text{O}$  hydrogen bonds are present (Figure 4(b)).

**3.5. Thermal Phase-Transition from the Black Phase into the Red One.** As judged from the heat of formation of the 2,9-DCIQA molecule (Table 2), the molecule in the red phase is, by far, more stable than that in the black phase. It is therefore expected that the black phase can be transformed into the red phase by heat treatment. In fact, the color change occurred from black via brownish red to vivid red by means of heat treatment in air at 300 °C for about 20 min. During this process, the shape of the crystals remained almost intact, while the surface morphology of the crystal changed noticeably, as shown in Figure 7 of the scanning electron micrograph. The present red crystal was also identified as the red phase by the X-ray analysis.

Furthermore, the heat flow was also observed as shown in the DSC curves (Figure 8) of the red and black crystals measured in air in the temperature range between 100 and 400 °C. A prominent exothermic peak was observed in the black phase in

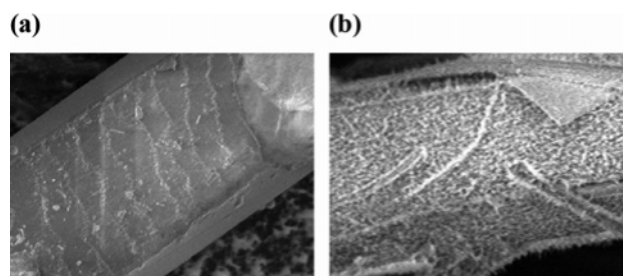


**Figure 7.** Scanning electron micrographs of the black needle: (a) before and (b) after heat treatment at 300 °C.

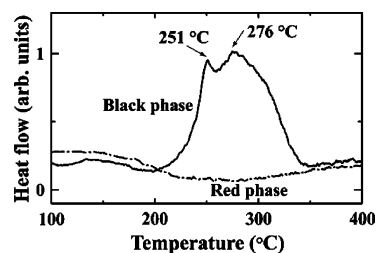


**Figure 8.** DSC curves measured on single crystals of the red phase (dash-dot line) and the black one (solid line).

the temperature region from about 200–340 °C, peaking at about 251 and 276 °C. The total exothermic energy amounts to about 237.8 J/g. The present exothermic energy supports directly the phase change from black to red.

#### 4. Conclusions

The conclusions drawn from the present investigation can be summarized as follows:

- (i) 2,9-DCIQA shows polymorphism: red and black phases. The former is the phase of the commercial product and corresponds to the high-temperature phase, whereas the latter is the low-temperature one.
- (ii) The molecule in the red phase is entirely planar. The molecules constitute a two-dimensional  $\text{NH}\cdots\text{O}$  hydrogen-bonded network. A large bathochromic shift occurs due to interactions between transition dipoles aligned in a “head-to-tail” fashion by means of the hydrogen bond.
- (iii) The molecule of the black phase is found to be heavily deformed and therefore much less stable than that of the red phase. The molecular distortion is also found to appreciably displace the absorption band toward longer wavelengths.
- (iv) The black phase is transformed into the red phase by heat treatment around 200 °C.
- (v) The structure of the red phase of 2,9-DCIQA and that of 2,9-DMQA is quite similar to each other. The only difference is found in the step height between hydrogen-bonded molecules. This induces a slight difference in excitonic interactions, leading to the difference in shade in the solid state.

#### References and Notes

- (1) Herbst, W.; Hunger, K. *Industrial Organic Pigments: Production, Properties, Applications*, 3rd ed.; VCH: Weinheim, Germany, 2004.
- (2) Mizuguchi, J.; Senju, T. *J. Phys. Chem. B* **2006**, *110*, 19154–19161.
- (3) Senju, T.; Sakai, M.; Mizuguchi, J. *Dyes Pigm.*, in press. [Online early access.] <http://dx.doi.org/10.1016/j.dyepig.2006.06.038>.
- (4) Mizuguchi, J. *J. Phys. Chem. A* **2000**, *104*, 1817–1821.
- (5) Mizuguchi, J.; Senju, T.; Sakai, M. *Z. Kristallogr. New Cryst. Struct.* **2002**, *217*, 525–526.
- (6) Mizuguchi, J.; Sasaki, T.; Tojo, K. *Z. Kristallogr. New Cryst. Struct.* **2002**, *217*, 249–250.

- (7) Senju, T.; Nishimura, N.; Hoki, T.; Mizuguchi, J. *Acta. Crystallogr.* **2005**, *E61*, o2596–o2598.
- (8) Senju, T.; Hoki, T.; Mizuguchi, J. *Acta. Crystallogr.* **2005**, *E61*, o1061–o1063.
- (9) Mizuguchi, J. *Cryst. Res. Technol.* **1981**, *16*, 695–700.
- (10) *Quantum CAChE*, version 3.2; Fujitsu, Ltd.: Kanagawa, Japan, 1999.
- (11) Ridley, J.; Zerner, M. *Theor. Chim. Acta* **1973**, *32*, 111–134.
- (12) Deuschel, W.; Honigmann, B.; Jettmar, W.; Schroeder, H. Quinacridone pigments. Great Britain Patent 923069, 1963.
- (13) Endo, A.; Matsumoto, S.; Mizuguchi, J. *J. Phys. Chem. A* **1999**, *103*, 8193–8199.
- (14) Mizuguchi, J.; Tojo, K. *J. Phys. Chem. B* **2002**, *106*, 767–772.
- (15) Mizuguchi, J.; Shikamori, H. *J. Phys. Chem. B* **2004**, *108*, 2154–2161.
- (16) Mizuguchi, J. *J. Phys. Chem. B* **2004**, *108*, 8926–8930.
- (17) Senju, T.; Mizuguchi, J. *J. Phys. Chem. B* **2005**, *109*, 7649–7653.
- (18) Kasha, M. Molecular Excitons in Small Aggregates. In NATO Advanced Study Institute Series, Series B; Bartolo, B. D., Ed.; Plenum Press: New York, 1976; Vol. 12; pp 337–363.
- (19) Craig, D. P.; Walmsley, S. H. Excitons in Molecular Crystals: theory and applications; W. A. Benjamin, Inc.: New York, 1968.